THE AERODYNAMIC AND STRUCTURAL DESIGN OF A VARIABLE CAMBER WING (VCW)

J P Fielding
S H M Macci
A V Mackinnon
J L Stollery

Cranfield Institute of Technology, Cranfield,
Bedfordshire, MK43 OAL
England

ABSTRACT

Current trends in the design of transport (civil/military) aircraft have shown that in order to be economically viable it is necessary to investigate technologies which may give an improvement in performance and operational flexibility. It is believed that the application of variable camber (VC) to a wing would assist in achieving such a goal.

With the aim of developing a system which satisfies the conflicting structural and aerodynamic requirements, investigations have been made to:-

1) Study the low and high speed theoretical and experimental aerodynamic effects of continuously changing the wing profile to suit all flight conditions.
2) Examine the practical (structural/mechanical) implications of applying such a concept to a real aircraft.

The two dimensional (chordwise) variation in camber is obtained by simultaneous rotation and extension of the trailing edge element near the aft region, and by simple droop of the leading edge (LE) element towards the front of the aerofoil. Thus a family of aerofoils of varying camber may be generated. Two dimensional experimental tests indicate that with increase in lift coefficient, gradual variation of camber results in lower drag compared with the basic undeployed section.
On a three dimensional wing it is necessary to divide the wing span into multi-segmented leading and trailing edge pieces. Experimental tests show that variation in spanwise lift distribution can be achieved if these spanwise segments are deployed independently. The root bending moment associated with gust loads or pilot initiated manoeuvre loads is significantly reduced by altering the spanwise lift distribution in such a way to cause inboard movement of the centre of pressure. This is achieved by selection of a highly cambered wing root portion combined with low or negatively cambered tip segments.

This paper:

1) Reports on the encouraging results found from the theoretical and experimental aerodynamic work,
2) Presents a design solution of a practical system which satisfies the aerodynamic requirements, and
3) Describes the tests carried out to verify the overall design concept.

Notation

LE - Leading edge
TE - Trailing edge
VCW - Variable Camber Wing
C_{TE} - Chordwise length of the trailing edge element
E - Youngs modulus of elasticity (N/mm^2)
C_L - Lift coefficient
C_{Lc} - Local lift coefficient
C_D - Drag coefficient
C_{Dinc} - Drag coefficient increment
C_{Rinc} - Roll coefficient increment
C_P - Coefficient of pressure
δ - Camber angle of rotation (Degrees)
α - Angle of incidence (Degrees)
η - Spanwise position of centre of pressure
$[90/0_2]_s$ - Orientation, No. and lay-up of carbon fibres. Subscript 's' refers to symmetric lay
[Note : all non dimensionalised coefficients are calculated based on the undeployed reference chord].

Segment No	1 Root	2	3	4 Tip	Symbol
Camber angle of rotation, δ (Degrees)	0	0	0	0	✳
	5	5	5	5	○
	10	10	10	10	◇
	5	5	0	0	□
	10	10	0	0	△
	5	5	0	-3.5	×

1. INTRODUCTION

The objective of this research was to investigate the problems and benefits of applying a variable camber wing (VCW) system to transport aircraft.

Spillman (Reference 1) pioneered a novel method of camber variation by means of rotation and translation of leading edge (LE) and trailing edge (TE) elements. The top surface was kept smooth and continuous to generate a family of cambered aerofoil sections. The proposal was tested experimentally by Rao (Reference 2) using a quasi two dimensional (2-D) wing. The work presented in this paper maintains the same deployment programme for the aft camber variation.

A supercritical aerofoil of 14 % thickness to chord ratio (t/cmax) was designed with generous section thickness between 50% and 70% chord and significant TE thickness. This was perceived to assist in accommodating the camber actuation equipment.

The details of the change in section profile are depicted in Figure 1. The position of maximum curvature on the upper surface lies at 64.5% chord and so was chosen as the junction between the centre body and the TE element. The origin of this curvature was selected as the centre of rotation and the camber angle, δ, was prescribed as the angle of rotation of the TE element in a circular arc about this origin. A flexible upper surface plate joins the centre body and the TE element to permit extension yet maintain curvature. The lower surface was a simpler system in which a rigid closing plate is hinged from the centre body at 60% chord and held by spring loads to the TE element. This geometry maintains a smooth top surface when deployed.

The purpose of LE deployment is to control the LE suction pressure peak caused by variations in circulation due to camber changes. Deployment of the LE element on a circular arc presented insurmountable design problems. These are overcome (see Figure 1) by simply drooping the LE element without extension, similar to the RAEVAM system. A description of this concept is given in Figure 2 (taken from Reference 3).

For a finite wing, spanwise variation of camber is possible by dividing the camber controlling devices into several segments along the span, each of which can be deployed independently. The geometric implications of achieving such a variation in wing camber are discussed in Section 3.2.

2. AERODYNAMIC DESIGN

2.1 VARIABLE CAMBER WING WIND TUNNEL MODEL

The variable camber (VC) half wing wind tunnel model shown in Figure 3 was of a rectangular planform swept at 25°. A semi-span distance of 1.6m and reference chord of 0.6m gave an aspect ratio of 5.33 which combined with a tunnel speed of 50 m/s resulted in a test Reynolds No. of two millions (2×10^6).

Discrete chordwise camber settings of -3.5°, 0°, 5° and 10° rotation were tested using detachable trailing edge (TE) pieces for each camber. The span was divided into four equal segments, thus any number of camber settings and spanwise positions could be achieved.
One TE piece of each camber setting was pressure tapped along with a leading edge segment and the centre body. The pressure distribution over the entire wing could therefore be measured by moving the appropriate pressure tapped segments along the span.

A series of tests was carried out with both uniform spanwise camber and discontinuous spanwise settings measuring forces and moments and recording pressure distributions at twelve spanwise stations.

2.2 FORCES AND MOMENTS

The notation used to describe the value of camber settings (rotation of the TE element about the origin) at each of the four span positions is simply done by stating the camber settings from root to tip (eg 10 10 0 0 describes a wing configuration of two 10 degree camber settings at the root portion combined with two undeployed settings at the tip).

Figure 4 displays the graph of lift coefficient (C_L) against incidence, α, for three uniform spanwise camber cases namely, 0°, 5° and 10°. Also shown are two cases with discontinuous spanwise camber settings , these being 10 10 5 5 and 5 5 0 0. It was found that the experimental lift curve slope of 3.86/rad compared well with the theoretical value of 3.87/rad (Reference 4) for the basic section. Subsequent increase in uniform camber across the span to 5° and 10° resulted in a parallel shift of the C_L vs α curve. Thus C_L at zero incidence rose from 0.092 to 0.342 for the 5° case and up to 0.646 for the 10° case.

The slope of both the discontinuous spanwise camber settings is greater than those of the uniform camber distribution. Examining the 5 5 0 0 case it would be expected that the lift against incidence curve would lie directly between that of 5° and 0° uniform case as the mean camber would be 2.5° across the span. These tests however show that for positive incidence the 5 5 0 0 lift against incidence curve lies nearer the 5° than the 0° curve. A similar pattern is repeated for the 10 10 0 0 case. This indicates that a large portion of the spanwise loading is carried by the segments at, or adjacent to the root of the wing.

Figure 5 shows the graph of drag coefficient against lift coefficient (C_D vs C_L) for the three uniform camber settings (namely 0° 5° and 10°). There appears to be little difference between the three curves but a trend can be seen. At low C_L an increase in camber results in an increase in C_D. As the C_L rises this drag difference reduces and at C_L of approximately 0.8 the drag of the 5° case equals that of the 0° case. Above this value of C_L it is seen that the more cambered sections produce less drag than the basic section. Thus at the higher values of C_L the C_D vs C_L curves overlap one another. To maintain the minimum drag the camber setting would have to be increased gradually with increasing C_L above 0.8.

To amplify the difference between these curves the drag increments with respect to the basic section, $C_{Dinc.}$ were plotted against C_L, as depicted in Figure 6. It is clearly seen that the higher the camber setting the larger the drag increment at zero lift. As C_L increases the drag increment for the 5° and 10° cases reduces. The 5° case matches drag with the basic section at C_L of 0.8 and the 10° case at C_L of 0.9. Above these values drag benefit is gained. Figure 6 also shows the drag increment for the aforementioned discontinuous camber cases plus a further case with the camber setting of 5 5 0 -3.5, which has two camber discontinuities across the span. For these three cases the reduction in drag increment with increased C_L is much sharper. For the configuration 5 5 0 0 the drag cross-over occurs at a C_L of approximately 0.42, whilst for the 10 10 0 0 case it occurs at a C_L of 0.8. This is a little

surprising as it was suspected that the configuration with mid-span camber discontinuity would generate additional vortex drag due to the geometry step between adjacent camber segments. However the reason is indicated by the spanwise lift distribution shown in Figure 11. With the spanwise change of camber (eg 5 5 0 0) the distribution is more nearly elliptic. The load distribution was further altered by introducing a second spanwise camber discontinuity with the configuration 5 5 0 -3.5. This condition results in almost the same drag as the 5 5 0 0 single camber discontinuity case.
In an attempt to reduce drag further, small fences were introduced between each of the TE segments to straighten cross flow. Over the entire C_L range the results show an extra drag increment due to the increased wetted area.

Figure 7 shows a graph of rolling moment coefficient increment with respect to the basic section, C_{Rinc}, against C_L. It demonstrates that little rolling moment change is experienced between uniform spanwise camber cases. This was to be expected as the planform remains rectangular and hence the spanwise loading are of similar shape. The 5 5 0 0 configuration shows a reduction in rolling moment coefficient of 20% at a C_L of 0.3 and further reduction is achieved with the 5 5 0 -3.5 and 10 10 0 0 configurations. This effect is more clearly shown in Figure 8, where the spanwise centre of pressure, η, is plotted against C_L. It is seen that the combination of large wing root cambers and low wing tip camber causes large inboard movements of the centre of pressure.

2.3 PRESSURE DISTRIBUTIONS

The pressure distributions were measured at twelve spanwise positions. From each chordwise distribution the local lift coefficient was calculated and as before was based on the reference chord.
Comparing the pressure distributions at spanwise station 7 (See Figure 9) for the three uniformly cambered wing cases identifies the need for an efficient and well controlled LE camber device. The rise in the LE suction pressure peak due to the increased circulation produced by the aft camber variation is significant. Early theoretical calculations confirmed the need for a LE device and a deployment method which maintained a smooth change in curvature, similar to that at the junction between the centre body and deployed TE element. It is also seen that significantly more aft loading results from the larger camber. This is due to the rotation and extension of the TE element and much of the additional lift is carried by the chord extension.
On the lower surface for the larger camber cases a discontinuity of slope of pressure coefficient, C_P, appears at 60% chord. This position is the joint between the hinged lower surface closing plate and the centre body and this peak was accepted in order to simplify the structural design. Theoretical calculations indicated negligible drag penalty which was insufficient to warrant modification.
Figure 10 shows the pressure distributions at stations 1, 7 and 12 for the uniform spanwise camber configuration 5 5 5 5 at zero incidence. It is seen that the root pressure distribution has a slightly lower LE suction peak compared to the mid-span pressure distribution at station 7. This is probably due to the existence of a small gap (3mm) between wing root and reflection plate to prevent rigging load interference. This gap allows a small passage of air from the lower surface to the upper surface reducing lift near the LE and increasing aft loading due to the presence of a small root vortex. At the tip of the wing C_L is zero and at station 12, 30mm from the tip, the pressure distribution is severely altered by the presence of the tip vortex. This increases the aft loading considerably and could be reduced by 'wash-out' near the tip. For a VCW this would be achieved by camber reduction of the tip segment.
It was found that the shape of the pressure distribution was similar for all the spanwise stations except station 12, the only difference being the gradual reduction of lift towards the tip. This suggested that the vortex influence was strongest over the outer 10 % of the span.
Figure 11 shows an almost rectangular spanwise lift distribution for the three uniform spanwise camber cases. Altering the spanwise camber by decreasing the tip camber and increasing the root camber changes the lift distribution significantly. This results in a large loss of lift in the outboard region. Consequently the centre of lift is moved inboard.

2.4 DISCUSSION

These results raised several points:

1) The C_L at which the uniform spanwise camber cases 5 5 5 5 and 10 10 10 10 cross-over in Figure 6 to indicate lower drag compared to the basic section are very high (greater than 0.8). The C_L range over which variable camber would be desirable would be between 0.2 and 0.6 for most civil aircraft at cruise. However theoretical calculations indicate that little more than 2° of camber rotation would be needed to cover this C_L range, therefore the 5° case would suit a high lift situation. The 10° case would be more applicable to the low speed take off and landing conditions where it is felt little or no additional assistance would be required from auxiliary high lift devices.

2) The selection of the origin of rotation based on the maximum curvature of the upper surface at 64.5% chord results in a large amount of chord extension for a given rotation. It is felt that the chord extensions of 13.6% and 27.7% for the 5° and 10° cases respectively are too great resulting in a large increase in the total wetted area. These values may be reduced by choosing an origin with a smaller radius of rotation resulting in more camber and less extension. The penalty for this would be a local increase in curvature on the upper surface at the junction between the centre body and the TE segment increasing the possibility of wave drag at transonic speeds.

3) The neglect of the LE camber deployment during wind tunnel tests results in large LE suction peaks. Whilst these may be tolerated to some extent at low speed the resulting wave drag at transonic speeds would be a severe penalty.

4) It is seen that spanwise variations of camber is a powerful tool for two reasons;

a) the rolling moment and hence the wing root bending moment can be significantly reduced by the deployment of large root cambers in conjunction with low tip cambers. Typically high lift manoeuvre situations would benefit greatly, as would the gust load alleviation problem.

b) The drag advantages of the 5 5 0 0 and 5 5 0 -3.5 configuration cases at C_L above 0.4 compared to the basic section indicates how the operational flexibility of a variable camber wing can allow the lift distribution to be altered to become more elliptic hence minimising vortex drag.

3. STRUCTURAL AND MECHANICAL DESIGN

3.1 TWO DIMENSIONAL (2-D) TRAILING EDGE (TE) DESIGN SCHEME

Aerodynamic investigations suggest that the predicted aerofoil performance improvements can best be achieved if the upper surface curvature is kept smooth and continuous. These geometric constraints therefore governed the practical, structural, and mechanical design of the VCW.

Figure 12 shows the essential features of the proposed scheme. It comprises of the following elements:

1) a solid trailing edge (TE) device,
2) a flexible upper surface,
3) a hinged lower surface,
4) an extending/conforming track,
5) a support track, and
6) a set of rolling elements for controlling the profile of the upper surface.

The necessary deployment curvature for the TE device is provided by attaching it to a curved extending track which slides within the support track of the same profile. The shape of these tracks is in keeping with the deployment arc A-B. Continuity between the TE device and the wing structure is provided by a flexible skin on the upper side and a hinged flap panel on the lower side. The flexible skin is clamped at the rear spar position and sits in a conforming track by means of a set of rolling elements. The conforming track is grooved in both the curved extending track and the TE device. It therefore matches the upper surface of the un-deployed TE device from point C to point D and curves from point C forward to match the shape of the extending track. The upper surface thus slides within the track during the TE deployment. The under side is kept continuous by means of a spring loaded lower surface closing plate hinged at 60% chord. Computational calculations showed no significant aerodynamic effects due to a slight kink at the lower surface hinge link.

The practical size of the upper surface skin restricts the range of deflection to either 0° to +10° or -3.5° to +7°. The position of the wing rear spar for the former range is 64.5% while for the later it is placed at 54%. The negative deflection was required for the flap to contribute to the roll control and wing root bending moment control.

3.2 THREE DIMENSIONAL (3-D) GEOMETRIC AND PRACTICAL DESIGN CONSIDERATIONS

Spanwise variation in camber is possible by dividing the control devices (LE and TE) into several segments similar to high lift devices on conventional wings. The resulting discontinuity between the differentialy deployed camber segments means that the motion should be in-line of flight. Figure 13a illustrates the planform arrangement of a typical transport aircraft wing, with the TE split in to six segments. The three inboard segments are deployed through positive angles only, while the three outboard segments have both positive and negative deflections. In reality this geometry is impossible to achieve for a swept and tapered wing, since the local radius of curvature varies along the span, increasing from tip to root. The deployment line joining the points of maximum curvature thus lies on a frustum of a cone.

If the segments are to move backwards in a line of flight direction with their edges streamwise, and at the same time rotate to give angular deflection, the axes of rotation, and the forward and aft end of the TE device must be unswept. The necessary changes to be made to the wing planform are shown in Figure 13b (the radius of curvature matches the outboard end of the segment). With such an arrangement the chord of the TE device, C_{TE}, (see Figure 12) decreases rapidly as the span of the segment increases.

From these arguments it is apparent that a true VC profile could only be achieved by placing the segments perpendicular to the hinge line and deploying them conically as shown in Figure 13c.

The conical nature of the deployment requires the support tracks to be attached at an angle to the vertical, as illustrated in Figure 13d (dashed lines). This angle is equivalent to the angle made by the segments to the line of flight. Such an arrangement gives a lateral movement to the TE device which is;

a) aerodynamically unsatisfactory; requiring large cover fairings (Figure 13c), and
b) structurally impossible to give differential deployment of adjacent segments.

The attachment of the tracks should be directly on to the wing structural box side ribs, as shown by full lines in Figure 13d. Deployment of a solid TE is obviously not possible with such an arrangement, unless the TE box is made to flex and warp or be supported by a suitable universal joint system.

It is apparent from Figure 12 that in order to have negative deflections the rear spar position must be moved forward (to 54% chord). If some of the segments were to have both negative and positive deployment while the rest only had positive deployment the rear spar must be staggered, as shown in the planform drawings of Figure 13. This is an obvious drawback since the structural efficiency of the system will be much lower than say the continuous spar arrangement. The structural efficiency is further reduced by introducing cutouts to allow the tracks to run in and out of the main wing section.

Most modern transport aircraft make use of the wing structural box for fuel storage. An obvious disadvantage of the proposed concept is the positioning of the tracks on the side ribs inside the wing box, thus invading the fuel space.

3.3 THREE DIMENSIONAL (3-D) STRUCTURAL MODEL DESIGN AND TESTING

From the above discussions it is clear that the key features of the design are:

1) The desire to have both conical and parallel deployment, and
2) The requirement for flexibility and controlled curvature of the upper surface.

It was decided therefore to design, construct and test a scaled prototype model of one TE segment with the following aims:-

a) Highlight the problems associated with a 3D deployment geometry.
b) Assess how the system (track/roller) behaves when actuated and deployed under applied loads.
c) Check the suitability of designing the upper surface with varying stiffness in span and chord.

The second and third objectives required the tracking system and the upper surface to be designed to meet suitable stiffness criteria.

3.3.1 Model Design

An illustration of the design of the proposed system is given in Figure 14.

Upper Surface Design

The design of the upper surface is critical to the whole concept. The most important aspect being spanwise stiffness and chordwise flexibility. The upper surface skin must have sufficient stiffness in order to hold shape without excessive warping due to the applied aerodynamic loads. At the same time flexibility along the chord is needed for it to conform without sticking and binding. The undesired warping can be prevented by any, or combination, of the following three ways:

1) The attachment of spanwise stiffeners across the chord of the upper surface,
2) The placement of several chordwise rails across the span,
3) The design of the surface in appropriate fibre reinforced plastic (FRP) material.

For the structural model it was decided to combine the second and third alternatives. The skin was made from carbon composite fibres and restrained along the chord at 5 segmental spanwise stations. The longitudinal (spanwise) and transverse E values of the material are 0.8175×10^5 N/mm^2 and 0.499×10^5 N/mm^2 respectively. The laminate is 2mm thick and has 8 (0.25 mm thick) plies orientated in $[90/0_2/+45/0_2/90]_s$ direction. The 0° plies are placed along the span to give chordwise flexibility.
The upper surface skin profile is changed through a series of tags (rolling elements) positioning the skin in strips (rails). At the inboard and outboard ends the rails are attached to the extending tracks and the TE device, while in the intermediate span position they are attached to the TE device only. On actuation of the TE device, the extending track moves aft, carrying the conforming strips. Thus the upper surface skin effectively slides within the aforementioned strips.
The design of the upper surface was based on a stiffness criterion which restricted the maximum deflection to be less than 2% of the maximum local spar depth. The deflection predictions were made using Finite Element (FE) analysis techniques by simulating face pressures on thin shell elements.

Tracking system

A two track system is adapted with an extending track sliding on top of a support track with the assistance of cam and needle rollers (See section drawing in Figure 14). The rollers are sized to react to aerodynamic loads, whilst the design of the tracks is based on their ability to transfer shear and bending loads to the support structure (wing box).

TE Device

Structural design of the TE was not necessary since its basic function was only to display the 3-D geometric problems associated with conical and parallel deployment of a solid body. It was therefore simply machined from laminated wood.

Actuation

Initially it was intended to have two actuators placed, one at either end of the segment. However such an arrangement can only be implemented if the TE device is made to flex along the chord and warp along the span. Since the TE device was designed as a solid body which was envisaged to experience a lateral movement during deployment, only a single actuator could be implemented. This actuator was placed in a mid-span position.

3.3.2 Structural Testing and Results

In view of the three test objectives, the testing had to be divided into three distinct phases:

Phase I - Stiffness testing of the upper surface and comparison of the results with the FE predictions.
Phase II - Observation of the TE deployment unloaded.
Phase III - Observation of the deployment with representative applied loads.

Phase I Testing

Verifications of the FE results could only be possible by testing the upper surface under similar loading conditions. Illustrations of the test apparatus is shown in Figure 15a. The test was carried out by supporting the upper surface on five chordwise formers along the span (simulating the tracks and conforming strips). The distributed load was applied by means of sand bags and the deflection measurements were made with dial gauges. 48 deflection measurements were recorded along the span and chord of the skin. An illustration of the measured and analysed deflections along the span at one chordwise station is given in Figure 15b. The miss-match of the results is due to slight miss

representation of the stiffness parameters and the loading between the two systems. In general the two sets of results correlate well with very little difference.

Phase II Testing

Once assembled, the TE was actuated in order to observe its translational motion. Figure 16 displays a photograph of the model in its maximum possible positive deployed position. Initial observations of the system suggested that the TE deployed smoothly. The upper surface was seen to conform smoothly and continuously without wrinkling or binding. The expected lateral movement across the span (from inboard to outboard) was evident. This was because of the different track radius at the two ends of the segment, which tends to twist the TE element. The TE element was obviously riding more on the larger radius (inboard) than it was on the smaller one.

The maximum measured extensions (for 7° of camber rotation) at the inboard and outboard ends were found to be approximately 270 mm and 261 mm respectively. In comparison the required extension at the two ends were 301 mm (inboard) and 264 mm (outboard). The difference in the two sets of figures implies that the TE device is too stiff to twist in order to flex for maximum parallel deployment. The TE device had a tendency to bind above 6° of deflection.

Phase III Testing

Figure 17 displays a photograph taken while operating the system under applied loads. The purpose of this exercise was to simply monitor the changes in deployment behaviour of the TE and the tracks due to applied loads. Observations indicated no real difference in the deployment of the loaded model in comparison with the unloaded model, except that the former system was much slower. This had been expected and is primarily due to rolling friction between the needle rollers and the two tracks.

3.4 DISCUSSION

A totally new design concept has been developed to satisfy the given geometric constraints of the aerofoil section and flap deployment set by aerodynamic requirements.

Extension of the concept to a 3-D wing showed how the desired conical and parallel deployments are possible only if a warping TE flap box or universal joints are used. This point is highlighted by designing the TE device of the structural model in laminated wood and operating under unloaded and loaded conditions. Deployment checks indicated no problems of achieving VC with continuous curvature tracks. The translational motions were observed to be smooth, and the upper surface flexed without wrinkling or binding.

FE analysis and initial static tests of the flexible upper surface suggest that it is possible to satisfy the stiffness requirements, provided that an appropriate number of chordwise rails are positioned along the span. The close proximity between the two sets of results indicates that much confidence can be placed in FE analysis, thus future work may not require separate stiffness checks for the upper surface.

4 RECOMMENDATIONS

1) The TE device structural box needs to be redesigned so that it flexes and has adequate stiffness such that it is not prone to flutter.

5 CONCLUSIONS

The outcome of this work was to design a variable camber wing which accommodates many of the conflicting structural and aerodynamic problems. The wind tunnel model demonstrated the possibility of improving the performance by means of both chordwise and spanwise camber variation. The structural model tested proved that such type of variation was a practical possibility.

ACKNOWLEDGEMENT

This project was a joint venture involving British Aerospace (Commercial Aircraft Division), the Department of Trade and Industry (DTI) and Cranfield Institute of Technology. It provided a unique opportunity to blend the extensive design experience of British Aerospace with Cranfield's research and testing facilities to produce a workable design solution. DTI's involvement was of great assistance to the aerodynamic design of the wind tunnel model and with its testing.

The authors wish to express their appreciation to all involved and especially to Professor J J Spillman, who originated the project and whose enthusiasm and experience contributed greatly to all aspects of the work.

REFERENCES

1) J. J. Spillman, The use of variable camber to reduce drag, weight and cost of transport aircraft. Aeronautical Journal, January 1992 Royal Aeronautical Society Paper No. 1844

2) A. J. Rao Variable camber wing for transport aircraft, PhD Thesis 1989 Cranfield Institute of Technology

3) Pierce and Treadgold A simple mechanical system to vary a wing section shape to suit various flight conditions. RAE TM 1149, 1969

4) Engineering and Science Data Unit (ESDU) ESDU Item 70011 - Lift curve slope and aerodynamic centre position of wings in inviscid

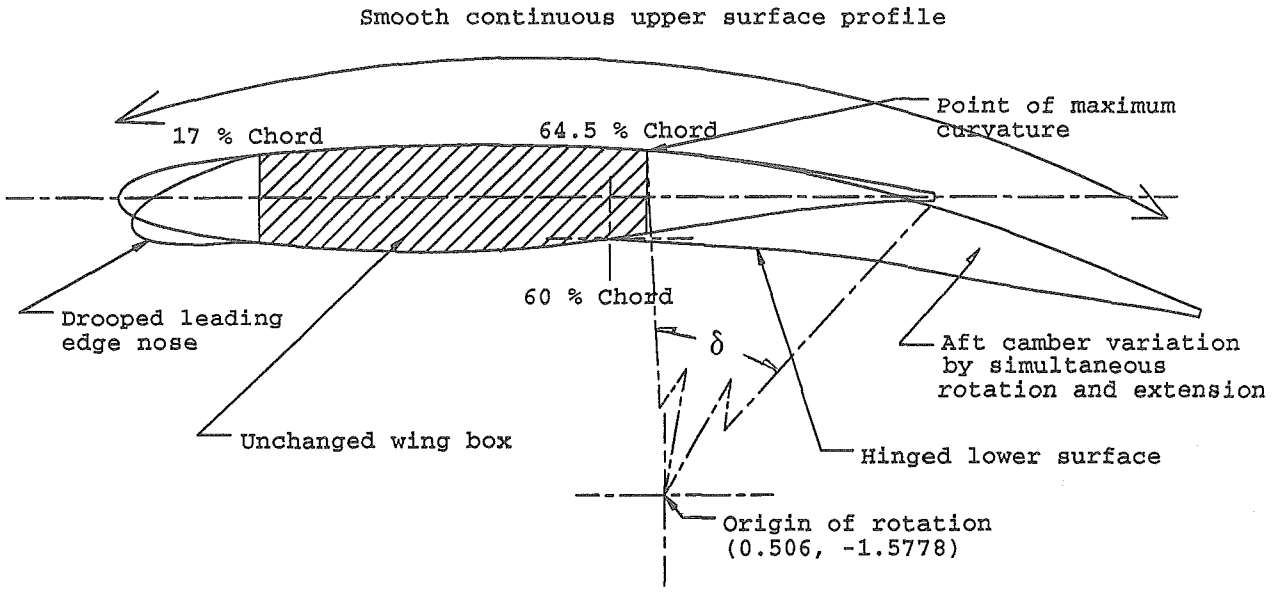

Figure 1: Basic aerofoil section indicating proposed camber variation scheme

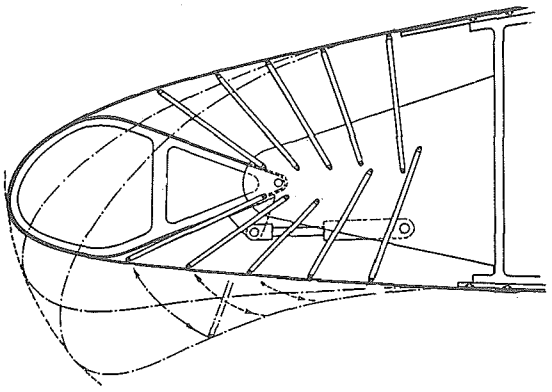

Figure 2: The RAEVAM leading edge droop

Segment No	1 Root	2	3	4 Tip	Symbol
Camber angle of rotation, δ (Degrees)	0	0	0	0	✳
	5	5	5	5	○
	10	10	10	10	◇
	5	5	0	0	□
	10	10	0	0	△
	5	5	0	-3.5	×

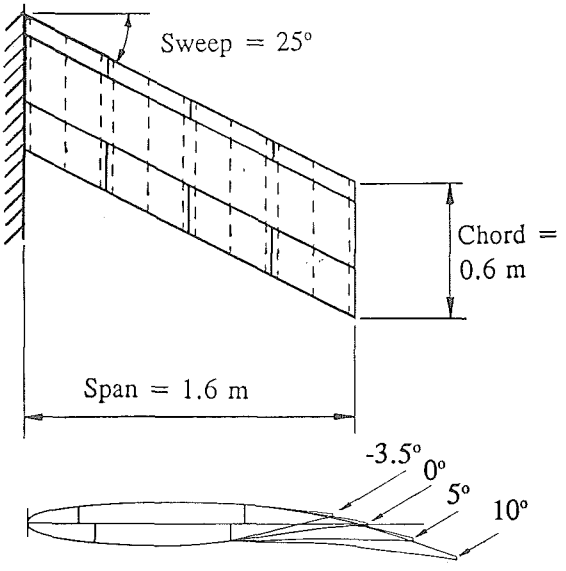

Figure 3: Four segment variable camber wind tunnel model

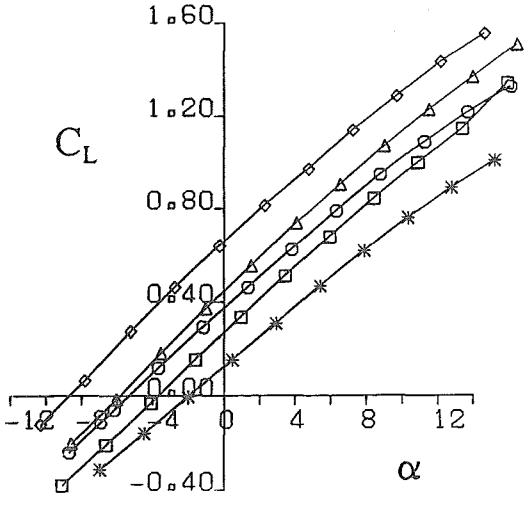

Figure 4: Lift coefficient vs Incidence

Segment No	1 Root	2	3	4 Tip	Symbol
Camber angle of rotation, δ (Degrees)	0	0	0	0	✳
	5	5	5	5	○
	10	10	10	10	◇
	5	5	0	0	□
	10	10	0	0	△
	5	5	0	-3.5	×

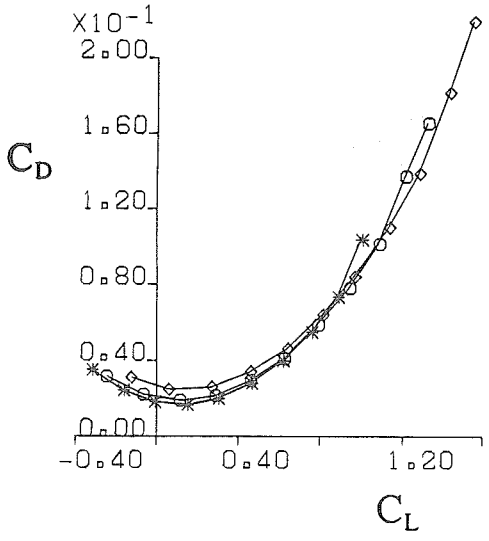

Figure 5: Drag coefficient vs Lift coefficient

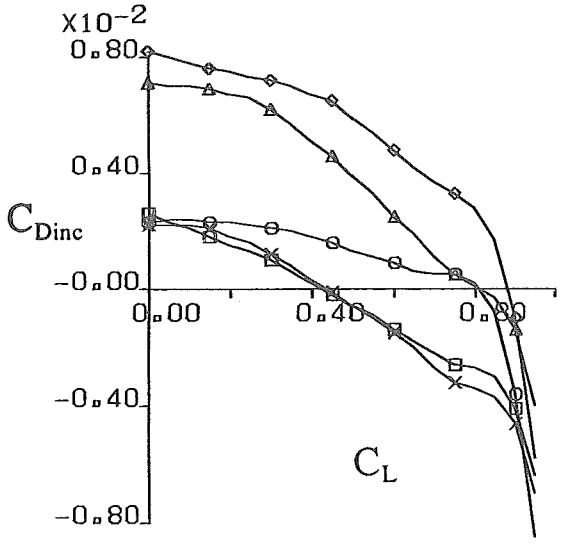

Figure 6: Drag coefficient increment vs Lift coefficient

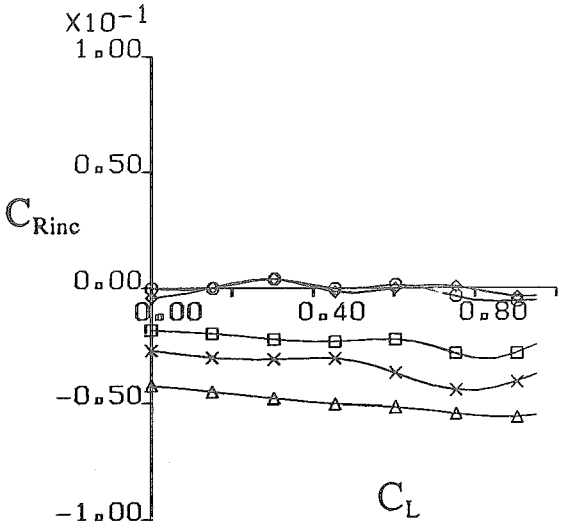

Figure 7: Roll coefficient increment vs Lift coefficient

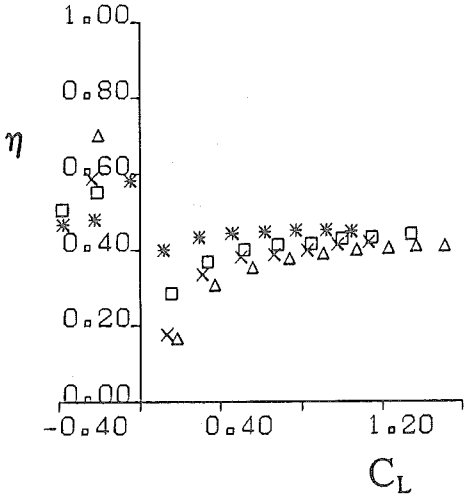

Figure 8: Spanwise centre of pressure vs Lift coefficient

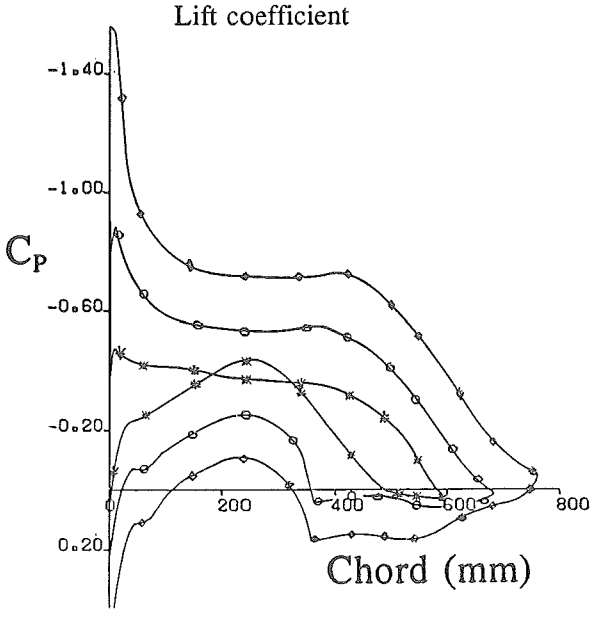

Figure 9: Pressure distributions at span station 7 for 0°, 5°, and 10° uniform spanwise camber

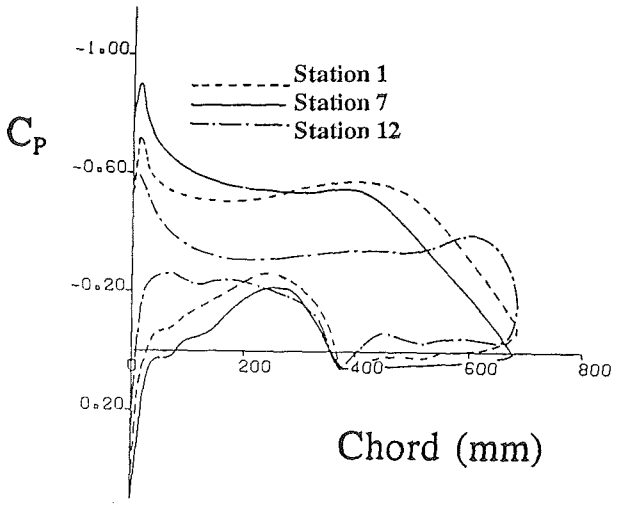

Figure 10: Pressure distributions at span stations 1, 7 and 12 for 5°, uniform spanwise camber

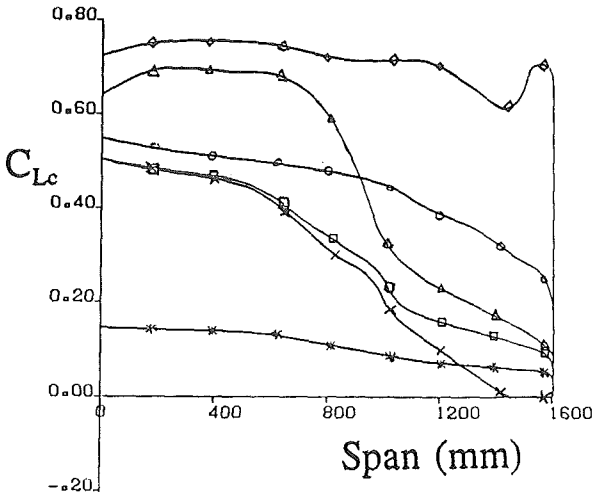

Figure 11: Spanwise lift distribution for various uniform and discontinuous spanwise camber

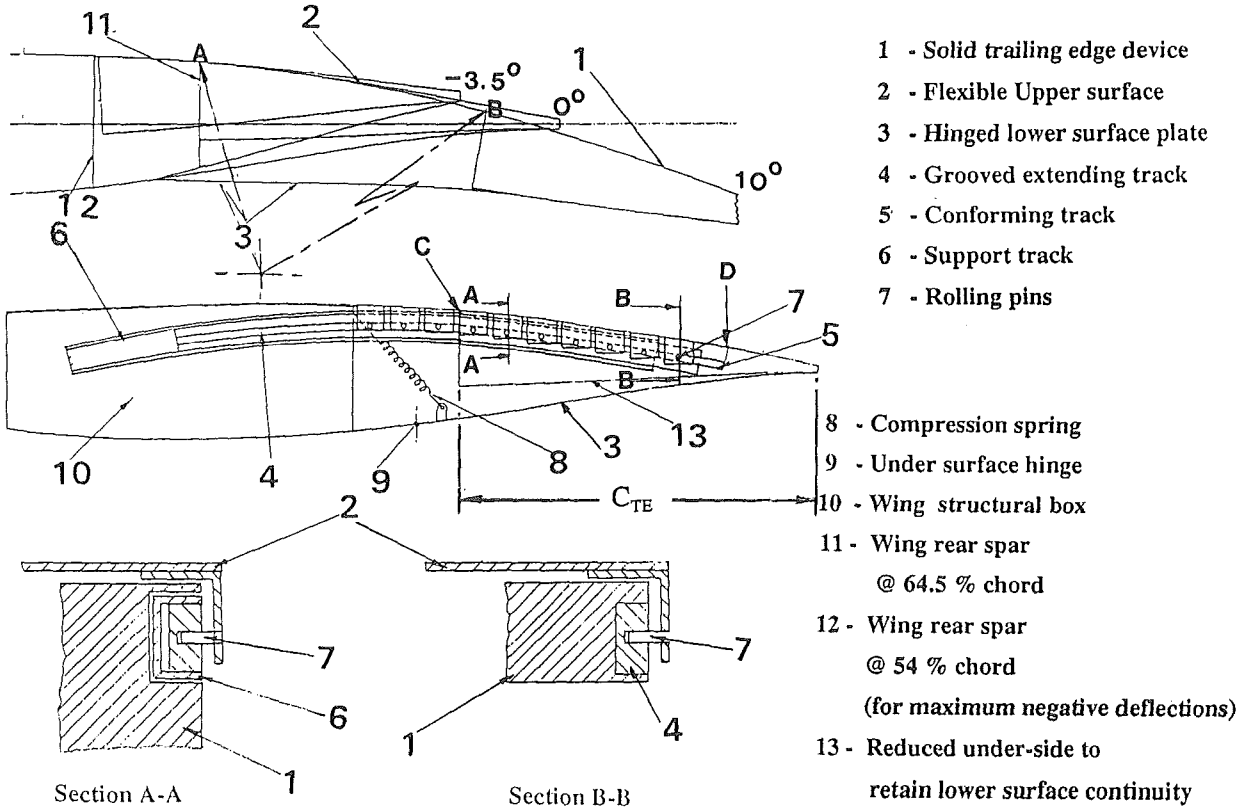

Figure 12: Two dimensional solution for aft camber variation

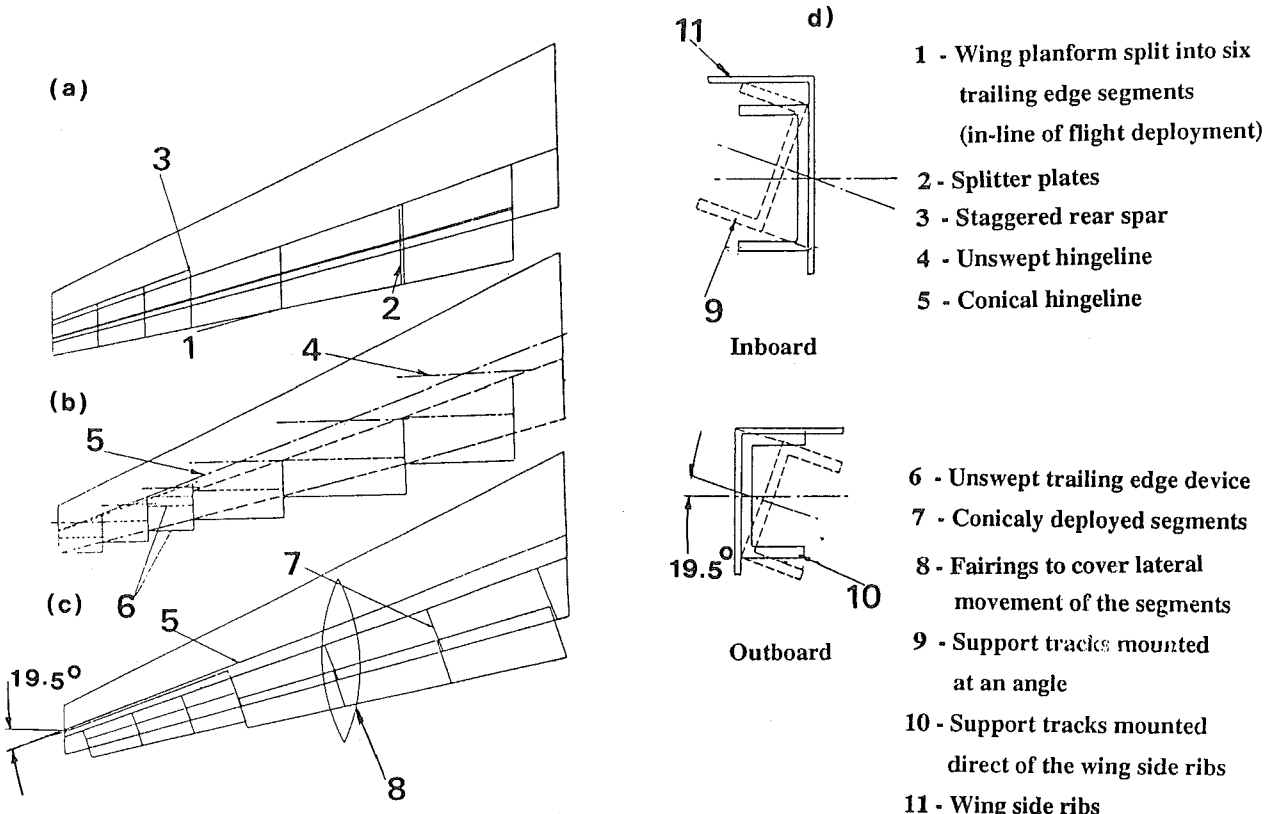

Figure 13: Three dimensional geometric implication of spanwise camber variation on a typical transport aircraft wing

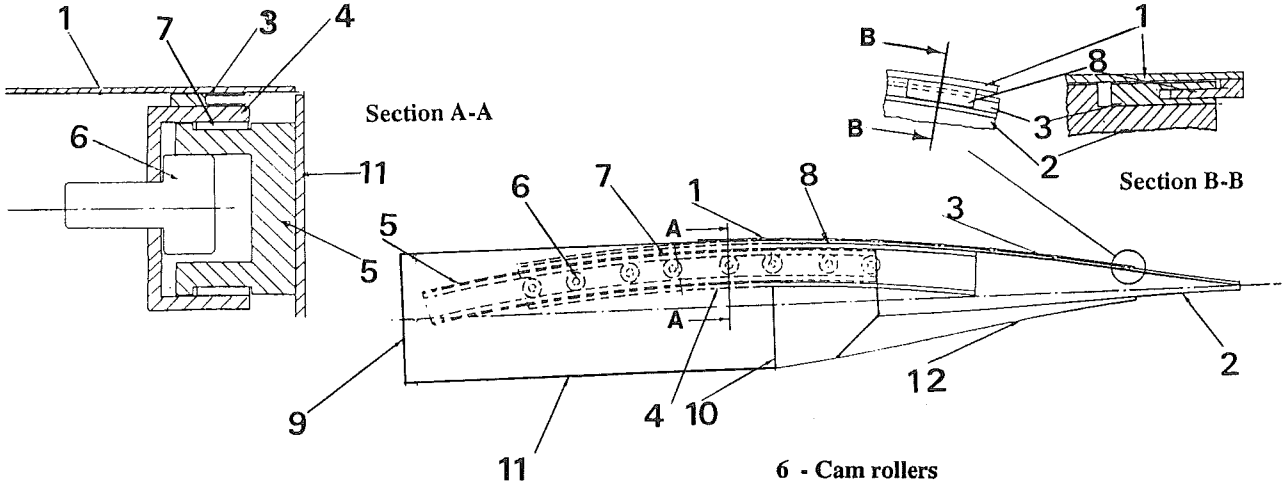

Figure 14: Three dimensional structural model

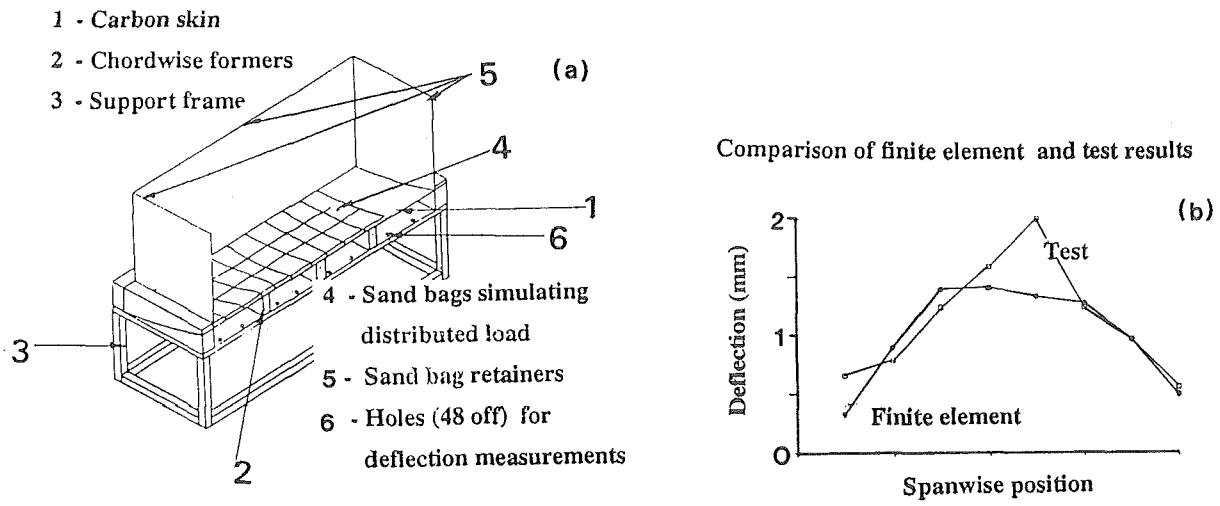

Figure 15: Static test arrangement and deflection measurements of composite flexible skin

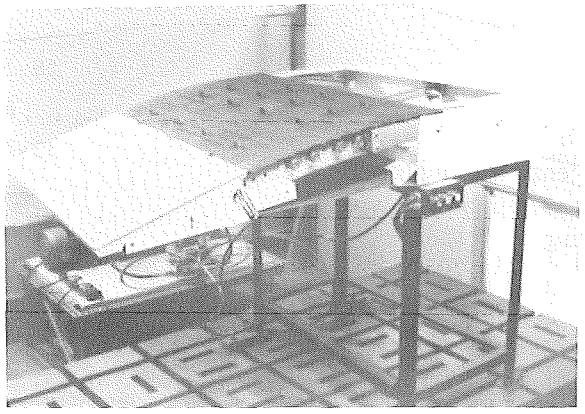

Figure 16: Photograph of model at maximum deployment

Figure 17: Operation of the structural model under applied load